TAO, Vol. 9, No. 4, 779-794, December 1998

Distribution of the Bottom-Simulating Reflector in the Offshore Taiwan Collision Zone

Wu-Cheng Chi[1], Donald L. Reed[2], Char-Shine Liu[3], and Neil Lundberg[4]

(Manuscript received 23 February 1998, in final form 31 August 1998)

ABSTRACT

A bottom-simulating reflector (BSR) has been identified in the offshore Taiwan accretionary prism using both migrated 6-channel and 120-channel reflection profiles. The BSR is marked by a reversed polarity reflector that increases in sub-bottom depth with increasing water depth, suggesting that the BSR marks the base of the methane hydrate stability field. The BSR is located in offscraped sediments derived from the Taiwan orogen and the Chinese continental margin, which may contain high amounts of organic carbon, thereby providing a source for the methane. Gas seepage found on land north of this region also supports the presence of methane in these strata. The BSR is typically located in the crests of anticlines and mud volcanoes, implying the migration and entrapment of methane gas. Recent uplift of the seafloor in anticlines may reduce pore pressure, thereby decomposing the hydrate phase into free gas, which may enhance the acoustic impedance contrast across the BSR. BSRs are conspicuously absent beneath submarine canyons in the region. A "flat spot" was found under the BSR within an anticline, suggesting that the hydrate-filled pore-space may result in lower sediment permeability, therefore enhancing the entrapment of free gas. We document the areal extent and sub-bottom depth of the BSR over a 77000 km^2-wide region around southern Taiwan. In particular at least 30% of the seafloor, to as much as 60%, along the trenchward slope of the accretionary prism is underlain by the BSR. The BSR is located at shallower sub-bottom depths on the trenchward (western) side of the accretionary prism than on the arcward (eastern) side, even though water depths are similar, implying enhanced fluid flow from depth, resulting in a higher geothermal gradient as sediments are accreted and dewatered along the Manila trench.

(Key words: Methane hydrates, Bottom-simulating reflectors, Convergent boundary, Multi-channel seismic reflection data)

[1] Department of Geology and Geophysics, University of California, Berkeley, CA, 94720, USA
[2] Department of Geology, San Jose State University, San Jose, CA, 95192-0102, USA
[3] Institute of Oceanography, National Taiwan University, Taipei, Taiwan, ROC
[4] Department of Geology, Florida State University, Tallahassee, Florida, 08544, USA

1. INTRODUCTION

A bottom-simulating reflector, or BSR (Figure 1), is a seismic reflector subparallel to the topography of the sea floor, which in some places cuts across reflectors generated by sediment layers (Shipley *et al.*, 1979). BSRs are commonly observed within several hundred meters of the sea-floor in continental slope sediments, particularly those associated with accretionary prisms (Hyndman and Davis, 1992). These seismic reflectors can be generated by the acoustic impedance contrast at the base of a sediment layer containing methane hydrate (Shipley *et al.*, 1979).

Methane hydrates influence a number of important submarine processes. For example, the hydrate, and any free gas trapped below, may provide a significant hydrocarbon resource in the future (Kvenvolden and McMenamin, 1980; Kvenvolden, 1993). Development of the offshore seabed may be influenced by seafloor instability and mass wasting, both of which are affected by hydrate formation and decomposition. The development of methane hydrate in accretionary prisms is affected by fluid flow, which also influences fault slip and potentially the seismic cycle (Moore and Vrolijk, 1992). Finally, methane hydrate in marine sediments may form a significant global sink of methane, an important "greenhouse" gas. Variations in bottom water temperature or the position of sea level may influence the stability of hydrate, and in some cases, could change the global methane storage in the atmosphere (Kvenvolden and McMenamin, 1980; Kvenvolden, 1993).

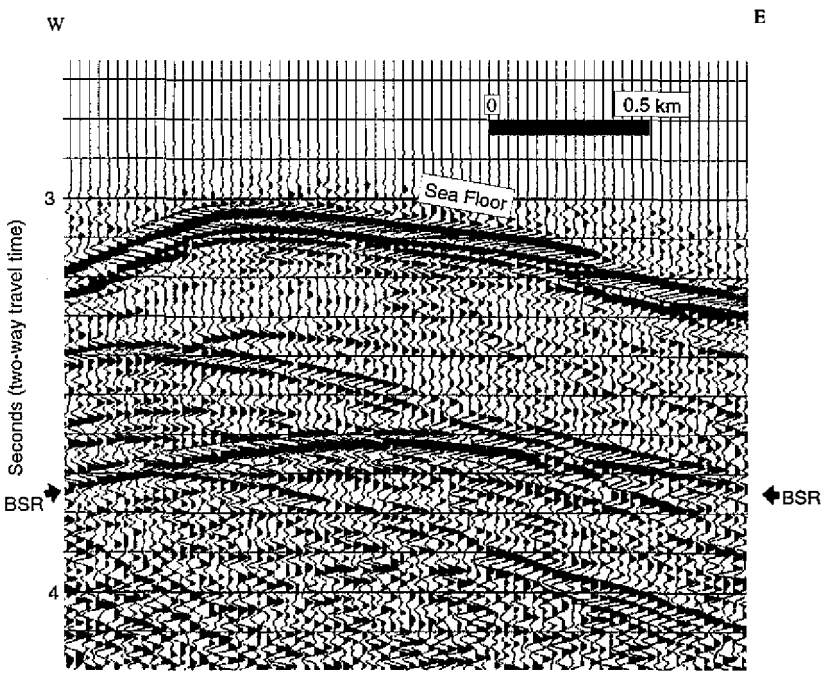

Fig. 1. Example of bottom-simulating reflector (BSR) with reversed polarity reflection located in anticlinal ridge. See site 1 on Figure 2 for location.

One of the challenges of methane hydrate research is to estimate the global distribution of this substance and its ability to store methane gas within or below the submarine hydrate layer. The identification of a BSR is one of the easier ways to detect the presence of methane hydrates and map their distribution, although hydrates have also been recovered in the sites without BSR (Holbrook *et al.*, 1996). Reed *et al.* (1991, 1992) first identified the presence of a BSR around southern Taiwan using 6-channel seismic reflection data. Subsequent studies have extended this work by identifying BSRs elsewhere around offshore southern Taiwan (Chi *et al.*, 1993; Hwang, 1993). Here we present the first comprehensive regional mapping of this submarine feature around southern Taiwan using a grid of migrated 6-channel and 120-channel seismic reflection profiles, the latter acquired in 1995 as part of the TAICRUST experiment. In addition, the location of the BSR will be compared to specific structural features along the seafloor in order to examine the potential factors leading to hydrate formation. A related paper on the implications of the distribution of the BSR to regional heat flow and fluid flow within the accretionary prism is in preparation.

2. PREVIOUS BSR STUDIES

Methane hydrates are "ice-like" clathrate structures in which methane molecules are enclosed within a solid lattice of water molecules. Most hydrates have been found in deep ocean sediments where there is a sufficient supply of methane and where pressure and temperature range between 0.2-5 MPa and 0-25 °C, respectively (Kvenvolden and McMenamin, 1980). The increase in temperature with depth below the seafloor, associated with the geothermal gradient, causes methane hydrate to become unstable and decompose at increasing sub-bottom depth, despite increasing pressure. As a result, the base of the methane hydrate defines a "phase boundary" separating the low-temperature stable phase of solid gas hydrate above from a field of instability below. The acoustic impedance contrast across the "phase boundary" can be large enough to generate reflections that are easily visible on seismic reflection profiles (Shipley *et al.*, 1979).

Kvenvolden (1993) has estimated that the total amount of methane in gas hydrate within marine sediments around the world is likely over 10^{19} g, consequently there is significant interest in this feature as a potential energy resource. The widespread abundance of methane hydrates in marine sediments also influences other geological oceanographic processes, including mass wasting and global climate pattern (Kvenvolden, 1993; Kvenvolden and McMenamin, 1980; McIver, 1977; Reed *et al.*, 1991; Paull *et al.*, 1996). For example, methane hydrate can act as cement, mechanically strengthening the sediments above the BSR, whereas unconsolidated sediment below the BSR may be more susceptible to mass failure and downslope movement. Thus a mechanical discontinuity is produced in marine sediments that could influence the location and distribution of submarine mass wasting. Moreover, any decrease in pore fluid pressure or increase in sub-seafloor temperature could decompose the bottom of the hydrate layer, thereby decreasing the ability of the sediment to withstand shear stresses. As a result, the sediment column becomes unstable and mass wasting may be enhanced. Using ^{14}C isotopic data from cores in the upper 7 m of the surface sediments. Paull *et al.* (1996) found that the glacial-age sediments in the gas hydrate field offshore the southeast-

ern United States are underrepresented in the core, in agreement with the prediction of increased frequency in mass wasting when hydrate is dissolved due to a lowering of sea level.

Decomposition of significant amounts of submarine methane hydrate can release methane, a greenhouse gas, into the atmosphere and global climate may be influenced. The amount of methane that is trapped in gas hydrates onshore and offshore is perhaps 3000 times the amount of methane in the atmosphere (Kvenvolden, 1993). Moreover, methane has a global warming potential 20 times larger than equivalent weight of carbon dioxide (Shine *et al.*, 1990). Global climate change, which can influence the position of global sea level and therefore the stability conditions of hydrate in the submarine environment, can impact the exchange of methane between the ocean and atmosphere. Prior to formulating models on the ocean-atmosphere exchange, we first need to have a better estimate of the global storage of methane in hydrates within marine sediments and a better understanding on the formation mechanisms of the hydrate. This study adds to the growing body of information documenting the distribution of methane hydrate around the world.

3. GEOLOGICAL SETTING OF TAIWAN COLLISION

The offshore Taiwan accretionary prism (Figure 2) is located on the boundary between the Eurasian plate and Philippine Sea plate where oceanic lithosphere of the South China Sea is subducting eastward beneath the Luzon island arc (Bowin *et al.*, 1978). The prism is bounded on the west by the Manila Trench, and on the east by the forearc basin of the North Luzon Trough (Hayes and Lewis, 1984). The Chinese continental margin enters the subduction zone near Taiwan and the subduction-related prism is modified by arc-continent collision (Suppe, 1981). Although the timing of initial collision is still under debate, it probably began in the late middle Miocene (Teng, 1990) and is currently propagating southward (Suppe, 1984).

The submarine accretionary prism contains three distinct structural domains (Figure 2) (Reed *et al.*, 1992): (1) a lower slope domain composed of mostly west-vergent ramp anticlines; (2) an upper slope domain with highly discontinuous reflections, suggesting intense deformation, and, possibly, out-of-sequence thrusting and underplating; and (3) a backthrust domain located along the rear of the prism. The North Luzon Trough, a forearc basin, is truncated in the region of collision by the juxtaposition of the rear of the prism against the volcanic arc along a region of backthrusting (Lundberg *et al.*, 1997).

4. SEISMIC DATA PROCESSING

This study is based on data acquired during a 6-channel seismic reflection survey conducted in 1990 aboard the R/V Moana Wave of the University of Hawaii and 120-channel seismic reflection survey in 1995 aboard R/V Maurice Ewing of Columbia University as part of the onshore-offshore seismic experiment known as TAICRUST (Figure 3). The 6-channel data were processed at UC Santa Cruz and San Jose State University using the SIOSEIS processing software with following sequence: debias correction, resample to 4 msec, spectral analysis, quality control, near trace gather, shot gathers, trace editing, geometry, AGC, spiking deconvolution, NMO, stack(4-fold), filter, predictive deconvolution, water-bottom mute, trace weighting, filter, AGC, stack section plot, F-K migration at 1500 m/sec, filter, AGC, and

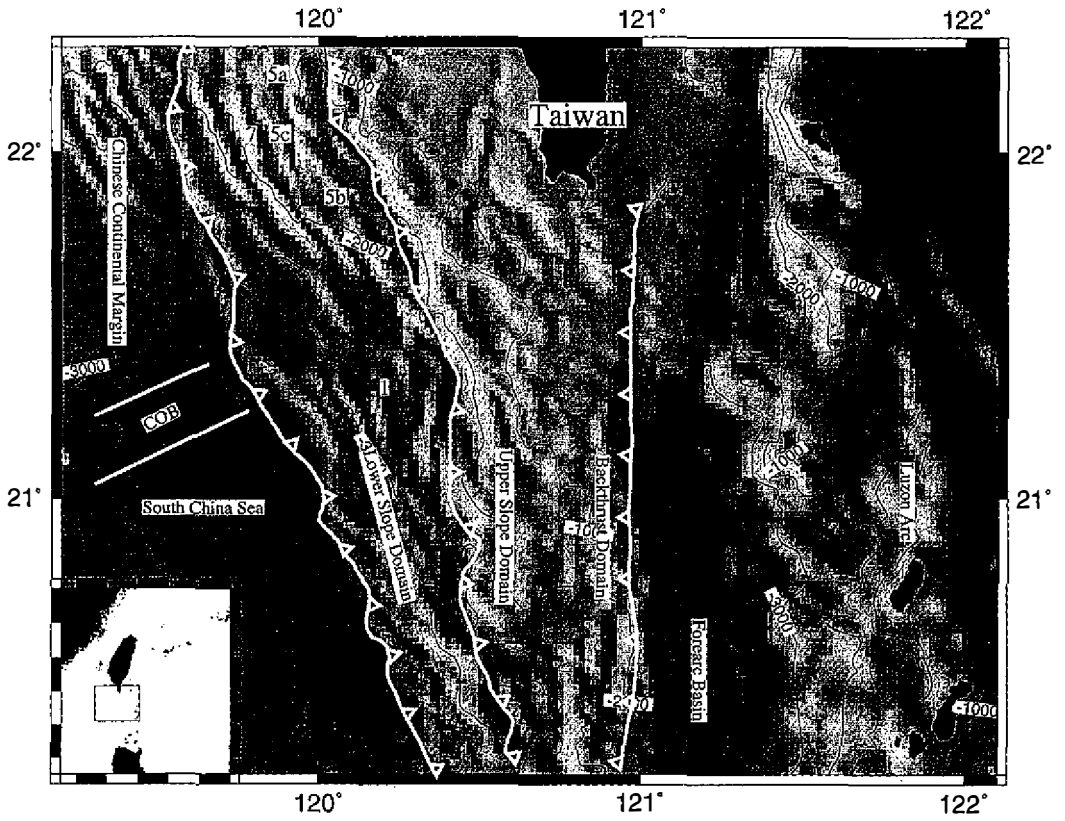

Fig. 2. Offshore tectonic framework map (after Reed *et al*, 1992). The basemap shows bathymetry of this region. Locations of seismic profiles in Figures 1, 5, and 7 noted as 1, 5a, 5b, 5c, and 7 respectively.

finally, migrated section plot (Reed *et al.*, 1992). The 120-channel reflection data were processed at University of Hawaii using ProMAX. This dataset, with large source-receiver offset and detailed interactive velocity analysis (0.6-1.2 km spacing) after DMO, provides good velocity information in this region, especially at shallow sub-bottom depths where BSRs are located. The velocity information is used to intially convert travel-times to subbottom depths for the BSR at several locations; more extensive conversion on a regional basis is planned for a future study.

5. DATA ANALYSIS

More than 8,000 kilometers of seismic reflection profiles, at an average spacing of 8 km, were examined over a region of 27,000 km^2 within the offshore Taiwan accretionary prism. We have made a determined effort throughout the study to separate reflectors associated with water-bottom reverberations from BSR identifications, for example shallow reflections marked by constant sub-bottom depths beneath a dipping seafloor reflection will be interpreted as

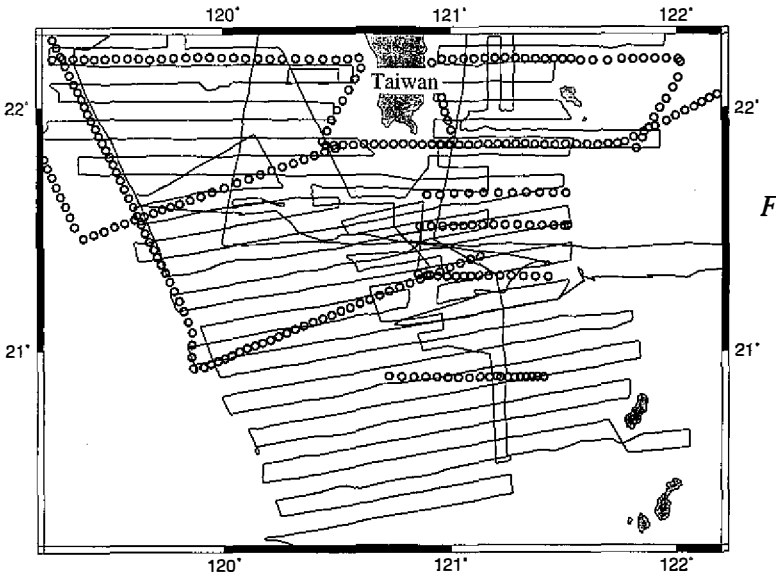

Fig. 3. Tracks of 1990 6-channel seismic data (solid lines) (after Reed *et al.*, 1992) and 120-channel seismic data associated with TAICRUST (dotted lines).

water-bottom reverberations, instead of a BSR. On these profiles, the BSR is identified as a reflector sub-parallel to the seafloor with reversed polarity. However, portions of the BSR may exhibit normal polarities where it is cross cut by bedding plane reflections. The BSR typically exhibits a single symmetrical pulse characteristic of a simple interface (Figure 1).

The BSR was identified at nearly 1,500 locations along the survey lines and each pick was assigned to one of three categories according to the confidence level of the identification (Q1, Q2 or Q3). These data were converted into methane hydrate distribution maps showing varying degrees of confidence in the accuracy of BSR identification (Figure 4). The BSR identifications with the highest confidence level compose the Q1 category with the following reflector characteristics: (1) subparallel to the seafloor in shallow sub-bottom depths, (2) reverse polarity with a single symmetrical pulse; and (3) a strong coherent reflection that cuts across bedding. The Q2 category or probable BSR identifications show similar characteristics to the Q1 picks except that the reflections are either segmented into pieces or may not cut bedding. The segment lengths of the Q2 reflectors are usually longer than the gaps between segments. The Q3 category, containing possible BSR picks, exhibits very weak and segmented reflections that are subparallel to the seafloor. BSRs in the Q3 group can be traced from adjacent Q1 or Q2 categories without abrupt changes in the subbottom depth.

6. STRUCTURAL RELATIONS OF BSR

BSRs are most commonly observed in the crests of anticlines (Figure 1). As a result of fault-related folding, followed by erosion of the seafloor or turbidite deposit, the seafloor is not parallel to bedding-plane reflections in these regions, thereby making the BSR easy to identify. The BSR usually has a larger radius of curvature as compared to strata within the anticline, resulting in subbottom depths of the BSR that are greater at the crest than along the

limbs of the fold. This local geometry of the BSR differs from regional BSR relation of increasing subbottom depth with increasing water depth.

The BSR was also found in many mud volcanoes and mud diapirs (Figure 5). The chaotic reflections within these features enhance the identification of BSRs. As in the anticlines, the BSR shows a gentle convex upward curvature. Shallower subbottom depths are observed underneath the crest of several volcanoes and diapirs, rather than on the limbs.

Many of the BSRs were also found in association with faults (Figure 5). At several locations in the lower slope domain, the BSR increases in amplitude in the forelimbs of fault-related folds. Many BSRs can be traced into the backlimbs of these folds, but disappear in flat-lying strata away from the fold, where the water depth becomes constant. We also found several places where the subbottom depth of the BSR decreases near the fault zones. However, we have not observed this relationship near fault zones in the upper slope domain. BSRs are not observed where the water depth changes abruptly, for example, in the bathymetric lows in submarine canyons.

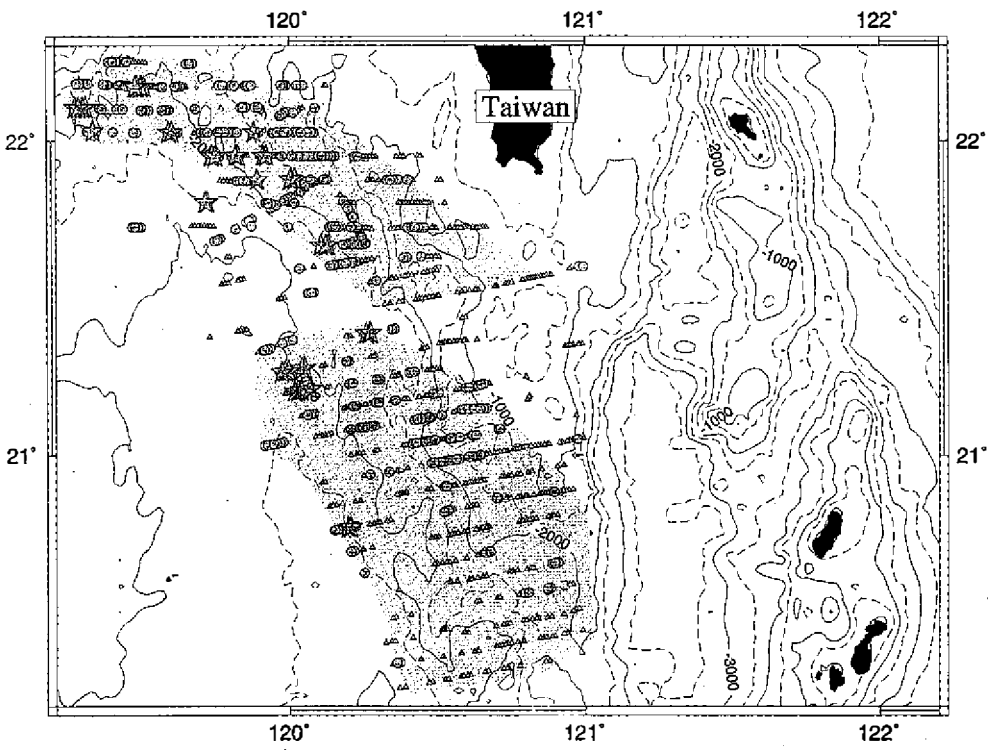

Fig. 4. Distribution of BSR identifications. Stars indicates Q1 class or highest confidence in BSR identification. Circles indicate Q2 class, or probable BSR identification. Triangles indicate Q3 class, or possible BSR identification. The two shaded areas are the two bathymetric highs that most BSRs are located.

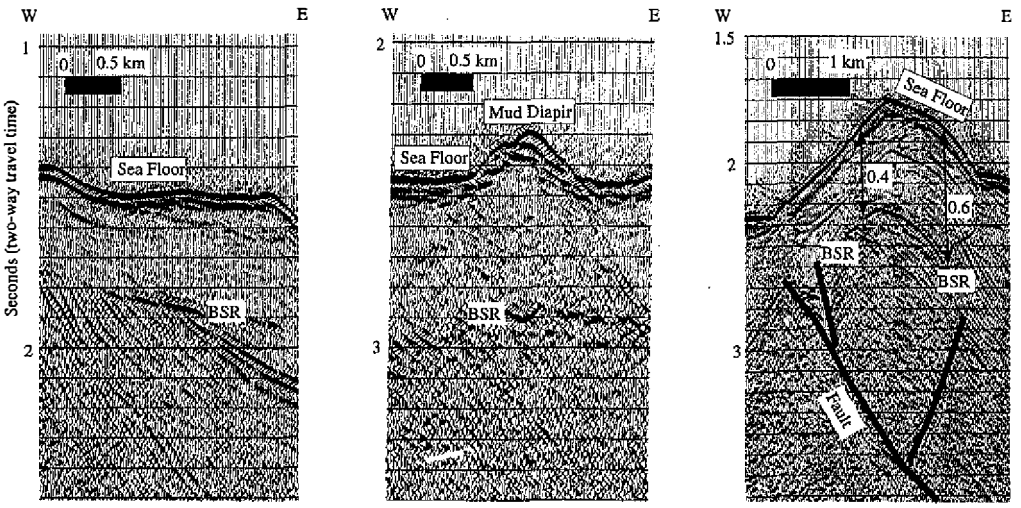

Fig. 5. Examples of BSR relations: a) sub-bottom depth increasing with water depth; b) shallowing beneath mud volcano, and c) shallowing toward fault zone despite increase in water depth. See Figure 2 for locations. Note the low reflection amplitude of the beddings above the BSR in 5a.

7. REGIONAL DISTRIBUTION OF BSR

The locations of the BSR were mapped across the forearc region between the Manila Trench and the North Luzon Trough (Figure 4). These maps clearly show the widespread occurrence of BSRs within the collision zone between water depths ranging from 800 to 3300 meters. The highest concentration of BSRs is located within the lower slope domain of the prism where sediments derived from the Chinese continental margin and Taiwan orogen are offscraped along the deformation front. The BSR was also identified in many regions of the upper slope domain and, in a few locations, in deformed forearc basin strata that have been incorporated into the rear of the prism by backthrusting. Several of the seismic lines associated with the TAICRUST experiment exhibit a BSR in the backthrust domain, some of which could not be identified in the coverage provided by the 6-channel dataset.

We have measured the distribution of the BSR identifications along seismic profiles in the region: Q1 and Q2 category BSRs cover more than 30% of the length of seismic profiles that cross the lower and upper slope domains, with the highest concentration in the collision zone. The majority of the Q1 and Q2 BSRs are within two large NW-SE trending bathymetric highs, each composed of several anticlines. BSRs of the Q3 category cover another 30% of the seismic profiles within the accretionary prism. The Q3 BSRs are concentrated along the rear of the prism. Combining all confidence level categories (Q1, Q2, and Q3), the BSR may extend across as much as 60% of the accretionary prism crossed by seismic profiles in this study.

Plots of water depth versus sub-bottom depth of the BSR were constructed (Figure 6). Two-way traveltime of BSR sub-bottom depth was converted into BSR sub-bottom depth in meters by using velocity-depth relations published by Hamilton (1980):

$$H_{BSR} = V_{avg} \times t$$

$$= [\, 1511 + (1041 \times t) - (372 \times t^2) \,] \times t$$

where: H_{BSR}: BSR sub-bottom depth, in m

V_{avg}: Average velocity of sediments above BSR, in m/sec

t: One-way traveltime of BSR sub-bottom depth, in sec

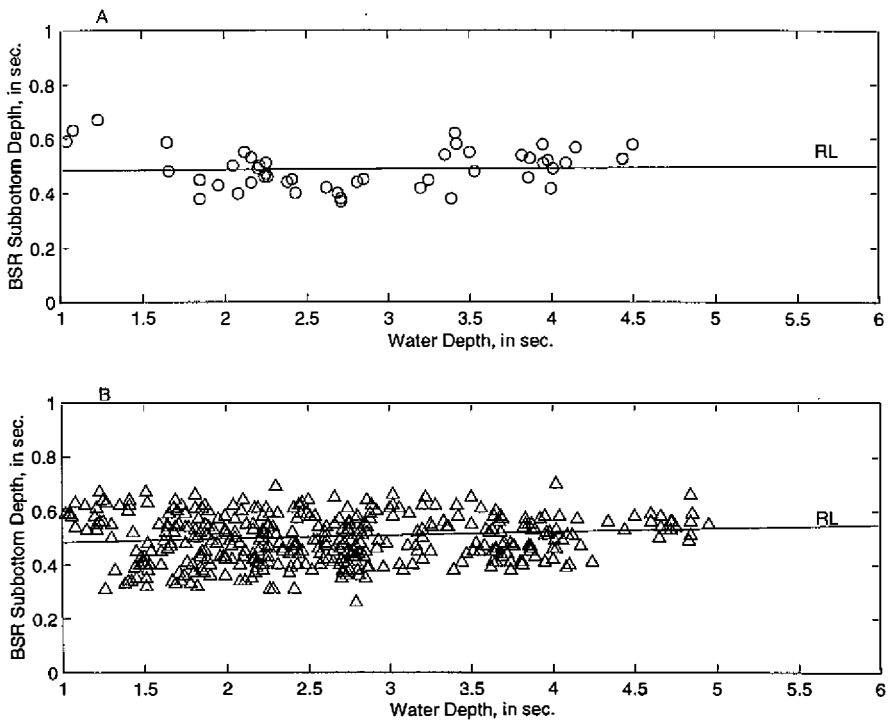

Fig. 6. a. Plot of Q1 subbottom depth against water depth. b. Plot of combined Q1 and Q2 subbottom depths against water depth. RL is the least-square line fit of the data.

This empirical equation does not consider velocity increases due to pore-filled hydrate. However, regions of hydrate in the Cascadia accretionary prism exhibit a velocity anomaly of less than 100 m/s (c.f. MacKay *et al.*, 1994). The average BSR sub-bottom depth is less than 0.5 sec (two-way traveltime) and, when combined with velocity variations of this magnitude, would result in a difference of less than 25 m in the sub-bottom depth conversion. Velocity information derived from Ewing data shows a similar velocity field, although the frequency range of the TAICRUST data (5-70 Hz) prevents us from resolving velocity structures smaller than a few tens of meters.

On all plots, the BSR is generally located at a sub-bottom depth of several hundred meters and increases in sub-bottom depth with increasing water depth (Figure 6). However, there is significant scatter in these plots caused in part by local decreases in the BSR sub-bottom depth near several fault zones, on the limbs of folds, and beneath mud volcanoes (Figure 5). The plot of the highest quality picks, or Q1 category, shows the least amount of scatter along a trend of increasing sub-bottom depth with increasing water depth. The combined plot of the Q1 and Q2 category data shows slightly more scatter around the general trend described above. Finally, the plot of all BSR picks (Q1, Q2, and Q3) shows the most amount of scatter.

8. DISCUSSION

Several lines of evidence indicate that the BSR around southern Taiwan represents the base of a methane hydrate stability field. First, the BSR in this region exhibits a reversed polarity reflection, suggesting a decrease in acoustic impedance across the BSR. This is a common observation of BSRs elsewhere in the world and is commonly attributed to the presence of patches of solid hydrate above the BSR and the absence of hydrate and/or presence of free gas trapped below (Shipley *et al.*, 1979; Miller *et al.*, 1991; Singh *et al.*, 1993; Bangs *et al.*, 1993; ODP Leg 146 Scientific Party, 1993; MacKay *et al.*, 1994; Scholl *et al.*, 1995; Dillon *et al.*, 1995; Wood *et al.*, 1995). Next, the BSR around southern Taiwan increases in sub-bottom depth with increasing water depth, implying that increasing hydrostatic pressures elevate the melting temperature of the hydrates. Consequently, the hydrate stability field is extended to greater subbottom depths before reaching temperatures high enough to result in decomposition. The BSR is widespread in areas of the accretionary prism composed of offscraped sediments of the Chinese continental margin and the Taiwan orogen, which may reflect high amounts of organic carbon in rapidly deposited terrigenous sediments deposited in the Manila Trench prior to accretion. Gas seepage has also been observed on land close to the study area (Central Geological Survey, 1996).

The common presence of BSRs in the crests of anticlines, mud volcanoes, and near the faults in the offshore Taiwan prism may be related to updip migration of gas and methane within folded strata. Very thick sedimentary sequences in the collision region are folded into long wavelength anticlines with the potential of tapping a very large volume of strata from which to derive methane. Gas can migrate upward within mud volcanoes, or even emit from them, as indicated by the onland mud volcanoes near this region (Central Geological Survey, 1996). The upward migration of warm fluids along faults or within mud volcanoes may have transported methane, either in a dissolved or free phase, into the crests of anticlines, and in-

crease the concentration of methane at shallow subbottom depths thus enhancing the generation of hydrate in the region. This process could also carry heat upward from depth thereby producing a shallowing of the BSR at fault zones as seen here and in the Casacadia accretionary prism (Zwart and Moore, 1993)

The highest concentration of BSRs is located in the northwest region of the study area (Figure 4) where offscraped terrigenous detritus derived from the Chinese continental margin and uplifted Taiwan orogen compose the lower slope domain of accretionary prism. The fine-grained fraction of rapidly deposited terrigenous sediments commonly has relatively high amounts of organic carbon, compared to pelagic sediment of the ocean basin (Selley, 1983). Organic carbon contained in offshore Taiwan strata may be the source of methane in the region, which has contributed to the formation of the hydrate layer. High concentrations of methane, either as free gas or dissolved in pore fluids, are required before hydrate can form. High sedimentation rates in this region may also suppress the escape of the solute into the water column (Hesse *et al.*, 1997). High concentrations of methane may ultimately become trapped in structural closures in the hinge zones of anticlines and hydrate formation itself may further assist in trapping methane in these regions.

The high amplitude and continuous nature of the BSR in the collision zone might also be affected by uplift in this area. Pecher *et al.* (1994) suggest that as strata are uplifted, the hydrostatic pressure on the base of methane hydrate layer will decrease, in respond to a decrease in overburden pressure associated with the overlying water column. As a result, the base of the hydrate layer will decompose into gas, which, if not dissolved, will then be trapped underneath hydrate layer, leading to an increase in the acoustic impedance contrast at the level of the BSR. This interpretation fits well with the observations in Taiwan, where the BSR is often located within the rapidly uplifting regions, such as the crests of the fault-bend folds, and on a larger scale, within the two NW-SE trending bathymetric highs. This mechanism may work in concert with the updip migration of methane gas to entrap free gas in the anticlinal ridges.

Many studies have suggested that free gas is trapped beneath the BSRs in other regions (Miller *et al.*, 1991; Singh *et al.*, 1993; Bangs *et al.*, 1993; ODP Leg 146 Scientific Party, 1993; MacKay *et al.*, 1994; Scholl *et al.*, 1995; Dillon *et al.*, 1995; Wood *et al.*, 1995). Direct hydrocarbon indicators in the form of high amplitude "flat spots" are found underneath the BSRs in several regions of the Taiwan prism (Figure 7), implying that the reduced permeability in hydrate-filled pore space may trap gas underneath methane hydrate stability field. Detailed velocity analyses of the long offset 120-channel data, acquired as part of the TAICRUST experiment, also found apparent low velocity zones below the BSR. A 50-100 m/s decrease in RMS velocity across the BSR observed in these data implies a greater decrease in interval velocity. In fact, velocity pull downs were identified in other locations, also suggesting the presence of free gas beneath the BSR. Recent vertical seismic profiling conducted during ODP Leg 184 on the Blake Ridge showed that low velocity zones may extend at 250 m beneath the BSR (Holbrook *et al.*, 1996).

In some areas of the Taiwan prism, reflection amplitudes decrease in the layer above the BSR (Figure 5). This "blanking" effect in the layer above the BSR has been observed in other regions around the world, including the Blake Ridge (Shipley *et al.*, 1979; Guerin and Goldberg,

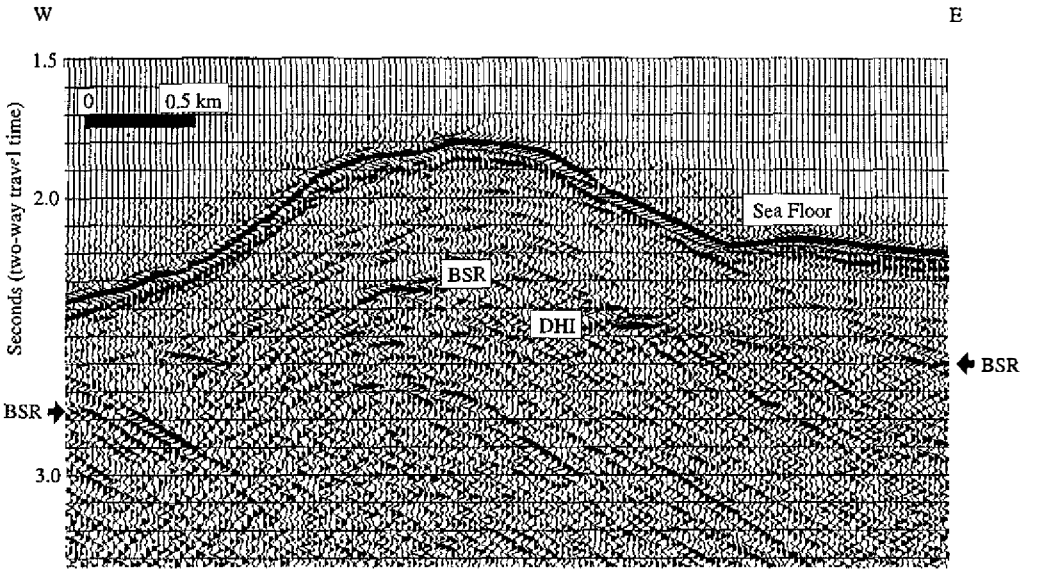

Fig. 7. Direct hydrocarbon indicator (DHI) underneath the BSR. See site 7 on Figure 2 for location of seismic profile.

1997) and Nankai Trough (Sakai, 1997). It is commonly attributed to the small magnitude of reflection coefficients within hydrate-bound sediments. The strong reflection amplitudes of the seafloor and BSR may also act to reduce the strength of reflections in these strata due to automatic gain control (AGC). However, we do not see higher amplitude bedding reflections at an equivalent sub-bottom depth where there is no BSR, implying that an AGC "shadow" from a high amplitude BSR does not change the amplitude of stratal reflections dramatically.

Detailed velocity analyses of Ewing data did not show a clear high velocity anomaly above the BSR that would be consistent with the enhanced rigidity and density in hydrate thereby producing an increase in the acoustic impedance contrast at the BSR. Also, we do not see any clear evidence of velocity pull up in those areas. These observations are similar to those of BSRs sampled at Blake Ridge (ODP Leg 146 Scientific Party, 1993), which show only small amount (< 15 % in bulk volume) of hydrates within the sediments. As a result, the mechanism for producing low amplitude reflections above the BSR is still unclear, and requires higher resolution geophysical/geochemical data and a better understanding of the elastic properties of hydrated sediments to be able to solve this problem.

In several regions we have made initial attempts at estimating the geothermal gradient from the BSR sub-bottom depth, methane hydrate phase equilibria, and seafloor temperature data following the method used by Ashi and Taira (1983). These calculations suggest a geothermal gradient ranging from 17 to 160 ^{o}C/km with most values between 25-45 ^{o}C/km. The geothermal gradient decreases eastward and shows similar results to the heat flow measurements conducted south of this region (Taylor and Hayes, 1983). Shyu *et al.* (this volume)

have conducted in-situ heat flow measurements within this region with 3 of the 4 measured geothermal gradients exceeding those derived from BSRs in nearby areas. However, one of the measurements shows excellent fit with the BSR-based geothermal gradients. Shyu *et al.* (this volume) have suggested that a 90% methane + 10% ethane gas composition in pure water yields a better estimate of the geothermal gradient in this region based on phase equilibria relations. Additional in-situ heat flow data are required to better calibrate BSR-derived estimates to seafloor measurements on a regional basis. A better knowledge of the fine scale velocity structures, history of seafloor temperature, and sediment thermal conductivity are necessary to use the BSR to estimate absolute heat flow values (Nissen *et al.*, 1995; Chi *et al.*, in prep.).

We can, however, compare the relative geothermal gradients at equivalent water depths on opposite sides of the accretionary prism in order to assess the potential role of fluid flow caused by sediment dewatering. MCS data from the TAICRUST program show shallower BSR subbottom depths along the western flank of the accretionary prism (Manila Trench) than on eastern side of the prism (North Luzon Trough). Line 33 of the TAICRUST program exhibits a high amplitude BSR at a subbottom depth of 0.52 sec at a water depth of 1275 m in the backthrust domain, which is located along the arcside of the accretionary prism. The BSR in the lower slope domain of the prism at the same water depth has shallower subbottom depth of 0.43 sec. Assuming that sediment velocity profiles, seafloor bottom water temperatures, and sediment thermal conductivity are similar at those two sites, the shallower BSR subbottom depth on the trench side suggests higher heat flow, which might relate to more intensive sediment dewatering leading to fluid flow from depth.

9. CONCLUSIONS

1. At least 20000 km^2 of the Taiwan accretionary prism is covered by a BSR, which is identified as a reflector sub-parallel to the seafloor with reversed polarity. Reversed polarity, increasing subbottom depth with increasing water depth, and the distribution of the BSR strongly suggests that this feature marks the base of the methane hydrate stability field.
2. The BSR is most commonly found in the crests of anticlines, mud volcanoes, and near the faults, which may relate to updip migration of free gas and methane dissolved in porefluids. Some of the gas might be trapped structurally, or beneath the hydrate layer.
3. The highest concentration of BSRs is located in the northwest region of the study area where rapidly deposited terrigenous sediments may have relatively high amounts of organic carbon, thereby providing a source for the methane.
4. Most of the Q1 and Q2 BSRs are located within the two NW-SE bathymetric highs in the lower slope domain. Uplift of the seafloor along these features will reduce the in-situ pressures, causing the base of hydrates to decompose. Consequently, released gas, trapped below the hydrate layer, might enhance the reflectivity of the BSR. Bright spots located underneath the BSR elsewhere in the prism suggest fluid migration and possible gas entrapment below the hydrate layer.
5. Geothermal gradients, estimated from the BSR sub-bottom depth, methane hydrate phase equilibria, and seafloor temperature data, range from 17 to 160 ^{o}C/km with most values

between 20-50 °C/km

6. Comparison of BSR subbottom depths on opposite sides of prism at the same water depth suggests elevated heat flow along the Manila trench, possibly due to sediment dewatering during accretion and fluid flow from depth.

Acknowledgments This work was supported by awards from the National Science Foundation of the USA (OCE-8911690, OCE-9314472, OCE94-16583) to D. Reed at San Jose State University. We thank Greg Moore for assistance in seismic data processing. We also thank captain and crew of R/V Moana Wave of the University of Hawaii and the captain and crew of R/V Maurice Ewing of Columbia University. C.T. Shyu is thanked for providing unpublished heat flow data. Reviews by Greg Moore and L. Teng helped improve the manuscript. Several figures were created using GMT graphic software (Wessel and Smith, 1995). The SIOSEIS processing system, developed by P. Henkart, was used to process and plot the seismic reflection data for this study.

REFERENCES

Ashi, J., and A. Taira, 1983: Thermal structure of the Nankai accretionary prism as inferred from the distribution of gas hydrate BSRs. *Geol. Soc. Am. Spec. Pap.*, **273**, 137-149.

Bangs, N. L. B., D. S. Sawyer, and X. Golovchenko, 1993: Free gas at the base of the gas hydrate zone in the vicinity of the Chile triple junction. *Geology*, **21**, 905-908.

Bowin, C., R. S. Lu, C. S. Lee, and H. Schouten, 1978: Plate convergence and accretion in the Taiwan-Luzon region. *Am. Assoc. Petrol. Geol. Bull.*, **62**, 1645-1672.

Central Geological Survey, 1996: Geological features of Taiwan, Vol. 2, edit by C.H. Chen, Central Geological Survey, Moea, Taipei, Taiwan, ROC, 171 pp.

Chi, W. C., D. L. Reed, N. Lundberg, and C. S. Liu, 1993: Distribution of the Bottom-Simulating Reflector in the offshore Taiwan collision zone: implications for fluid migration (abs.): Eos, Trans, AGU, Fall Meet., Suppl., 74, 583.

Dillon, W. P., R. M. Drury, D. F. Coleman, and M. W. Lee, 1995: Geological factors that concentrate gas hydrate on a passive continental margin, Eos Trans, AGU, Spring Meet. Suppl., 76, 163.

Guerin, G., and D. Goldberg, 1997: Characterization of in situ elastic properties of hydrated sediments, Eos Trans, AGU, Spring Meet. Suppl., 78, F339.

Hamilton, E. L., 1980: Geoacoustic modeling of the sea floor. *J. Acoustical Soc. America*, **68**, 1313-1340.

Hayes, D. E., and S. D. Lewis, 1984: A geophysical study of the Manila trench, Luzon, Philippines, 1. *Crustal structure, gravity, and regional tectonic evolution*, **89**, 9171-9195.

Hesse, R., P. Egeberg, and S. K. Frape, 1997: Chlorine-isotopic evidence for long-range diffusion in Blake Ridge submarine gas-hydrate field: ODP leg 164 results, Eos Trans, AGU, Spring Meet. Suppl., 78, F339.

Hwang, Y. L., 1993: Geological structural analysis offshore southwestern Taiwan. Master thesis, Institute of Oceanography, National Taiwan University, 58pp .(in Chinese)

Holbrook W. S. H. Hoskins, R. A. Stephen, D. Lizarraide, W. T. Wood, Leg 164 Science Party: 1996: Methane hydrate and free gas on the Blake Ridge from Vertical Seismic profileing, ODP Leg 164, Eos Trans, AGU, Spring Meet. Suppl., 77, F323.

Hyndman, R. D., and E. E. Davis, 1992: A mechanism for the formation of methane hydrate and seafloor Bottom-Simulating-Reflectors by vertical fluid expulsion. *J. Geophys. Res.*, **97**, 910-924.

Kvenvolden, K. A., 1993: Subaquatic gas hydrate occurrence—models and settings: Eos, Trans, AGU, Spring Meet., Suppl., 74, 369.

_____, and M. A. McMenamin, 1980: Hydrates of natural gas: a review of their geologic occurrence, U.S. Geological Survey Circular, 825, 1-11.

Lundberg, N., D. L. Reed, C. S. Liu, and J. Lieske, Jr., 1997: Forearc-basin closure and arc accretion in the submarine suture zone south of Taiwan. *Tectonophysics*, **274**, 5-23.

Mackay, M. E., R. D. Jarrard, G. K. Westbrook, R. D. Hyndman, and the Shipboard Scientific Party of ODP Leg 146, 1994: Origin of Bottom Simulating Reflector: geophysical evidence from the cascadia accretionary prism. *Geology*, **22**, 459-462.

McIver, R. D., 1977: Hydrate of natural gas: important agent in geologic processes, GSA Abstra. Programs, 9, 1088-1090.

Miller, J. J., M. W. Lee, and R. von Huene, 1991: An analysis of a seismic reflection from the base of a gas hydrate zone, offshore Peru. *American Assoc. Petrol. Geolog. Bull.*, **75**, 2204-2213.

Moore, J. C., and P. Vrolijk, 1992: Fluids in accretionary prisms. *Rev. Geophys.* **30**, 113-135.

Nissen, S. S., D. E. Hayes, B. Yao, W. Zeng, Y. Chen, and X. Nu: Gravity, heat flow, and seismic constraints on the processes of crustal extension: Northern margin of the South China Sea. *J. Geophys. Res.*, **100**, 22447-22483.

ODP Leg 146 Scientific Party, 1993: ODP Leg 146 examines fluid flow in Cascadia Margin, Eos, Trans, AGU, Spring Meet., Suppl., 74, 345.

Paull, C. K., W. J. Buelow, W. Ussler III, and W.S. Borowski, 1996: Increased continental-margin slumping frequency during sea-level stand above gas hydrate-bearing sediments. *Geology*, **24**, 143-146.

Pecher, I. A., T. A. Minshull, S. C. Singh, and R. von Huene, 1994: The formation of free gas beneath the hydrate stability zone offshore Peru: Evidence from reflection seismic data, Eos, Trans, AGU, Fall Meet., Suppl., 75, no. 44, 672.

Reed, D. L., N. Lundberg, C. S. Liu, K. D. McIntosh, J. H. Jr. Lieske, and B. Y. Kuo, 1991: Strain domains, fluid/gas migration and protothrusting in the offshore Taiwan accretionary wedge (abs.), Geological Society of America, Abstracts with Programs, 23, 365.

Reed, D. L., 1990: Relations between mud volcanoes, thrustdeformation, slope sedimentation, and gas hydrate, offshore North Panama. *Mar. Petrol. Geol.*, **7**, 44-54.

Reed, D. L, N. Lundberg, C. S. Liu, B. Y. Kuo, 1992: Structural relations along the margin of the offshore Taiwan accretionary wedge: implications for accretion and crustal kinematics. *Acta Geologica Taiwanica*, **30**, 105-122.

Sakai, Akio, 1997: Seismic studies related to gas hydrates offshore Japan, Eos, Trans, AGU,

Fall Meet., Suppl., 78, no. 46, f344.

Scholl, D. W., A. J. Stevenson, and P. E. Hart, 1995: Eocene formation of the Bering Sea Basin linked to regional-scale tectonism of Alaska- implications for energy gas resources and the accumulation of massive hydrate deposits (VAMPs), Pacific Section Convention, 18.

Selley, R. C, 1983: Petroleum geology for geophysicists and engineers. International Human Resources Development Corporation, Boston, 87pp.

Shine, K. P., 1991: Climatic effects of carbon dioxide and methane releases. *Teaching Earth Science*, **16**, 17-20.

Shipley, T. H., and B. M. Didyk, 1982: Occurrence of methane hydrates offshore southern Mexico, Initial Reports of the Deep Sea Drilling Project, 66, 547-555.

Shipley, T. H., M. H. Houston, R. T. Buffler, F. J. Shaub, K. J. McMillen, J. W. Ladd, and J. L Worzel, 1979: Seismic evidence for widespread possible gas hydrate horizons on continental slopes and rises, American Association of Petroleum Geologists Bulletin, 63, 2204-2213.

Singh, S. C., T. A. Ninshull, and G. D. Spence, 1993: Velocity structure of a gas hydrate reflector. *Science*, **260**, 204-207.

Shyu, C. T., S. K. Hsu, and C. S. Liu, 1998: Heat Flows off Southwest Taiwan: Measurements over Mud Diapirs and Estimated from Bottom Simulating Reflectors. *TAO*, **9**, 795-812.

Suppe, J., 1981: Mechanics of mountain building and metamorphism in Taiwan. *Memo. Geolog. Soc. China*, **4**, 67-89.

Suppe, J., 1984: Kinematics of arc-continent collision, flipping of subduction, and back-arc spreading near Taiwan. *Memo. Geolog. Soc. China*, **6**, 21-33.

Taylor, B., and D.E. Hayes, 1983: Origin and history of the south China Sea basin, AGU,.*Geophys. Monogr.*, **27**, 23-56.

Teng, L.S., 1990: Geotectonic evolution of late Cenozoic arc-continent collision in Taiwan, *Tectonophysics*, **183**, 57-76.

Wessel, P., and W. H. F. Smith, 1995: New Version of the Generic Mapping Tools Released, Eos Trans, AGU, Suppl., 76, no 17, 329.

Wood, W. T., Rowe, M. M., and J. F. Gettrust, 1995: Very high resolution 2-D seismic modeling of the base of methane hydrate in the Blake Ridge, Eos Trans, AGU, Spring Meet., Suppl. 76, 164.

Zwart, G., and J. C. Moore, 1993: Variations in temperature gradient of the Oregon accretionary prism: Eos, Trans, AGU, Spring Meet., Supple., 74, 222.